Inorganic Chemistry

Article

pubs.acs.org/IC

Effect of Axial Ligands on the Spectroscopic and Electrochemical Properties of Diruthenium Compounds

Machima Manowong,[†] Baocheng Han,*[,‡] Thomas R. McAloon,[‡] Jianguo Shao,[§] Ilia A. Guzei,[∥] Siyabonga Ngubane,[⊥] Eric Van Caemelbecke,[†,#] John L. Bear,[†] and Karl M. Kadish*[,†]

[†]Department of Chemistry, University of Houston, 112 Fleming Building, Houston, Texas 77204-5003, United States

[‡]Department of Chemistry, University of Wisconsin—Whitewater, 800 West Main Street, Whitewater, Wisconsin 53190-1790, United States

[§]Department of Chemistry, Midwestern State University, 3410 Taft Boulevard, Wichita Falls, Texas 76308, United States

[∥]Department of Chemistry, University of Wisconsin—Madison, 1101 University Avenue, Madison, Wisconsin 53706-1322, United States

[⊥]Molecular Science Institute, School of Chemistry, University of the Witwatersrand, Johannesburg, Wits 2050, South Africa

[#]Department of Chemistry, Houston Baptist University, 7502 Fondren Road, Houston, Texas 77074-3298 United States

Supporting Information

ABSTRACT: Three related diruthenium complexes containing four symmetrical anionic bridging ligands were synthesized and characterized as to their electrochemical and spectroscopic properties. The examined compounds are represented as $Ru_2(dpb)_4Cl$, $Ru_2(dpb)_4(CO)$, and $Ru_2(dpb)_4(NO)$ in the solid state, where dpb = diphenylbenzamidinate anion. Different forms of $Ru_2(dpb)_4Cl$ are observed in solution depending on the utilized solvent and the counteranion added to solution. Each Ru_2^{5+} form of the compound undergoes multiple redox processes involving the dimetal unit. The reversibility as well as potentials of these diruthenium-centered electrode reactions depends upon the solvent and the bound axial ligand. The $Ru_2^{5+/4+}$ and $Ru_2^{5+/6+}$ processes of $Ru_2(dpb)_4Cl$ were monitored by UV−vis spectroscopy in both CH_2Cl_2 and PhCN. A conversion of $Ru_2(dpb)_4Cl$ to $[Ru_2(dpb)_4(CO)]^+$ was also carried out by simply bubbling CO gas through a CH_2Cl_2 solution of $Ru_2(dpb)_4Cl$ at room temperature. The chemically generated $[Ru_2(dpb)_4(CO)]^+$ complex undergoes several electron transfer processes in CH_2Cl_2 containing 0.1 M $TBAClO_4$ under a CO atmosphere, and the same reactions were seen for a chemically synthesized sample of $Ru_2(dpf)_4(CO)$ in CH_2Cl_2, 0.1 M $TBAClO_4$ under a N_2 atmosphere, where dpf = *N*,*N*′-diphenylformamidinate anion. $Ru_2(dpb)_4(NO)$ undergoes two successive one-electron reductions and a single one-electron oxidation, all of which involve the diruthenium unit. The CO and NO adducts of $Ru_2(dpb)_4$ were further characterized by FTIR spectroelectrochemistry, and the IR spectral data of these compounds are discussed in light of results for previously characterized $Ru_2(dpf)_4(CO)$ and $Ru_2(dpf)_4(NO)$ derivatives under similar solution conditions.

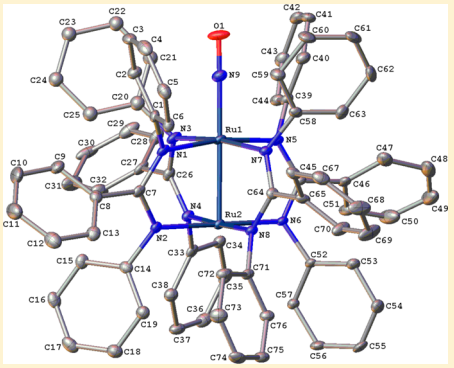

INTRODUCTION

The structural, electrochemical, and spectroscopic properties of numerous diruthenium complexes with a Ru_2^{5+} core and a paddle-wheel structure have been reported in the literature[1−27] since the first synthesis and physical characterization of $Ru_2(OAc)_4Cl$ (OAc = acetate anion) by Stephenson and Wilkinson in 1966.[28] The majority of investigated Ru_2^{5+} complexes have contained an axially bound chloride anion and are formulated in their neutral form as Ru_2L_4Cl or $Ru_2(OAc)_x(L)_{4-x}Cl$ (x = 1−4) where L is a symmetrical or unsymmetrical anionic bridging ligand.[1,6,8,16,18,19,21,24−26,29,30]

Four redox reactions are generally observed for these types of diruthenium compounds in nonaqueous solvents such as CH_2Cl_2, benzonitrile (PhCN), or acetonitrile (CH_3CN). The electrode reactions are almost always reversible and correspond to one-electron additions or one-electron abstractions at the dimetal unit as described in eqs 1−4.

$$Ru_2^{5+} + e^- \rightleftarrows Ru^{4+} \quad (1)$$

$$Ru_2^{4+} + e^- \rightleftarrows Ru^{3+} \quad (2)$$

$$Ru_2^{5+} \rightleftarrows Ru^{6+} + e^- \quad (3)$$

$$Ru_2^{6+} \rightleftarrows Ru^{7+} + e^- \quad (4)$$

The $E_{1/2}$ values for reduction and oxidation of the diruthenium unit will depend upon the type and number of anionic bridging ligands as well as upon the type and number of

Received: March 31, 2014
Published: July 8, 2014

   dx.doi.org/10.1021/ic5007605 | *Inorg. Chem.* 2014, 53, 7416−7428

axial ligands which could be anionic or neutral. For example, the $E_{1/2}$ for reduction of $Ru_2(F_5ap)_4Cl$ in CH_2Cl_2 was reported as −0.35 V,[23] where F_5ap = 2-(2,3,4,5,6-pentafluoroanilino)-pyridinate anion while $Ru_2(ap)_4Cl$ is reduced at −0.87 V versus SCE[17] under the same solution conditions, a difference of more than 500 mV with changes in substituents on the ap bridging ligands (where ap =2-anilinopyridinate anion). Likewise, the $E_{1/2}$ for reduction of $Ru_2(ap)_4CN$ is located at −0.73 V while $[Ru_2(ap)_4(CN)_2]^-$ is reduced at −1.24 V in the same solvent,[31] again a difference of more than 500 mV in $E_{1/2}$ for the $Ru^{5+/4+}$ process with change of axial ligands.

Changes in the type of axial ligand, while maintaining the same number and type of bridging ligands, not only will affect the redox potentials as described above but also may lead in some cases to a change in electronic configuration and/or chemical reactivity of the diruthenium complexes in their various dimetal oxidation states.[13,32,33] Indeed, $Ru_2(dpf)_3(OAc)(BF_4)$ where dpf = *N,N′*-diphenylformamidinate anion was shown to exist as a quantum admixture of spins whereas $Ru_2(dpf)_3(OAc)Cl$ exists only in an S = 1 spin state.[13] The reaction of CO with $Ru_2(dpf)_3(OAc)(BF_4)$ (or most likely $[Ru_2(dpf)_3(OAc)]^+$ in solution) was shown to afford the mono-CO adduct, $[Ru_2(dpf)_3(OAc)(CO)]^+$, whereas no reaction at all is seen between $Ru_2(dpf)_3(OAc)Cl$ and carbon monoxide which does not bind to the Ru_2^{5+} form of the examined compound.[33]

In earlier studies from our laboratory we have reported how systematic changes in the bridging ligands would affect redox potentials of the dimetal unit,[8,17,34] and we have now turned our attention to systematically investigating the effect of neutral and anionic axial ligands on the redox potentials of a series of Ru_2^{5+} compounds with the same four anionic bridging ligands. The investigated diruthenium compounds are represented as $Ru_2(dpb)_4X$, $[Ru_2(dpb)_4X_2]^-$, and $[Ru_2(dpb)_4]^+$ (dpb = diphenylbenzamidinate anion) where X is a neutral or negatively charged axial ligand or a solvent molecule. The redox reactions given by eqs 1−4 were examined in CH_2Cl_2 and PhCN containing a variety of added anions, and the products of each electron addition or electron abstraction were characterized by cyclic voltammetry combined with thin-layer UV−vis and IR spectroelectrochemistry.

EXPERIMENTAL SECTION

General Procedures and Reagents. Ultra-high-purity grade nitrogen gas (N_2), nitric oxide (NO), and research purity grade carbon monoxide (CO) were purchased from Matheson Trigas or Praxair. Both N_2 and NO were passed through anhydrous calcium sulfate and sodium hydroxide pellets to eliminate traces of water prior to use while CO was used without further purification. Tetra-*n*-butylammonium perchlorate ($TBAClO_4$, Fluka Chemicals Co.), tetra-*n*-butylammonium hexafluorophosphate ($TBAPF_6$, Sigma-Aldrich), tetra-*n*-butylammonium fluoride (TBAF, Fluka Chemicals Co.), tetra-*n*-butylammonium chloride (TBACl, Fluka Chemicals Co.), tetra-*n*-butylammonium iodide (TBAI, Sigma-Aldrich), and tetra-*n*-butylammonium bromide (TBABr, TCI America) were all used as received without further purification. Dichloromethane (CH_2Cl_2, 99.8%, EMD Chemicals) was used as received whereas PhCN (Sigma-Aldrich) was distilled over P_2O_5 under vacuum before use.

Physical Measurements. Cyclic voltammetry was carried out with an EG&G model 263A potentiostat by using a three-electrode system made up of a glassy carbon or platinum disc working electrode, platinum wire counter electrode, and a homemade saturated calomel electrode (SCE) as the reference electrode. A fritted glass bridge was used to separate the SCE electrode from the supporting electrolyte/solvent mixture. UV−vis measurements were recorded on a Hewlett-Packard model 8453 diode array spectrophotometer using cells with path lengths of 10, 1, 0.1, and 0.01 cm, the exact value depending on concentration. Infrared spectroelectrochemistry experiments were carried out using a Nicolet 6700 FT-IR spectrometer by Thermo Scientific. A homemade three-electrode cell, whose design has been reported in the literature,[35] was used for spectroelectrochemistry experiments. The IR spectra of each electrooxidized or electroreduced complex under N_2 were obtained as difference spectra measured against the corresponding unoxidized or unreduced compound. Mass spectra were recorded using an electrospray ionization (ESI-MS) or MALDI-TOF mass spectrometer at the University of Houston Mass Spectrometry Laboratory. Elemental analysis was carried out by Atlantic Microlab, Inc., Norcross, GA. Ferrocene (Fc) was used as internal standard in the electrochemical studies; the $E_{1/2}$ of the Fc/Fc^+ couple in CH_2Cl_2 with 0.1 M $TBAClO_4$ was measured as 0.48 V versus SCE.

Calculation of Formation Constants by UV−Vis Spectroscopy. Changes of the UV−vis spectra of $Ru_2(dpb)_4Cl$ in CH_2Cl_2 containing 0.1 M $TBAClO_4$ were monitored during a titration with PhCN, and the resulting spectral data then used to calculate the formation constant using the Hill equation (see eq 5)[36]

$$\log[(A_i - A_0)/(A_f - A_i)] = \log K + n \log[\mathrm{PhCN}] \quad (5)$$

where A_i is the absorbance in solutions with a specific concentration of added PhCN, A_0 is the initial absorbance where [PhCN] = 0.0 M, and A_f is the final absorbance of the coordinated species. The slope of the $\log[(A_i - A_0)/(A_f - A_i)]$ versus log [PhCN] plot gives n, the number of PhCN species bound to the diruthenium center, and the value of log K is evaluated from the intercept of the line at log [PhCN] = 0.0.

Calculation of Formation Constants by Electrochemical Titration Method. Change in half-wave potentials for reduction or oxidation of $Ru_2(dpb)_4Cl$ in CH_2Cl_2 containing 0.1 M $TBAClO_4$ were monitored during a titration with PhCN in order to calculate the formation constants for ligand binding using eq 6

$$(E_{1/2})_c = (E_{1/2})_s - 0.059 \log \frac{K_{MLp}}{K_{(MLq)^-}} - (p - q)0.059 \log[L] \quad (6)$$

where $(E_{1/2})_c$ and $(E_{1/2})_s$ are half-wave potentials for the ligated and unligated diruthenium compound, and p and q are equal to the number of ligands bound to the oxidized and reduced forms of the compound. K_{MLp} and $K_{(MLq)^-}$ are the formation constants of the ML_p and $(ML_q)^-$, respectively. When the ligand concentration is equal to 1.0 M or when $p = q$, the difference in half-wave potentials between $(E_{1/2})_c$ and $(E_{1/2})_s$ will directly give the ratio of stability constants for binding of an axial ligand to the two different oxidation states of the redox couple.

Synthesis of Starting Materials. Diruthenium acetate, $Ru_2(OAc)_4Cl$,[28] and *N,N′*-diphenylbenzamidine (Hdpb)[37] were prepared following procedures reported in the literature.

$Ru_2(dpb)_4Cl$ (1). In a round-bottom flask, $Ru_2(OAc)_4Cl$ (1.9 g, 4.03 mmol) was added to *N,N′*-diphenylbenzamidinate (50.0 g, 184 mmol) and heated (>170 °C, 10 h) under vacuum (10^{-2} mm Hg) to melt the ligand. The unreacted *N,N′*-diphenylbenzamidinate ligand was sublimed (12 h) from the reaction mixture under vacuum (160 °C at 10^{-2} mm Hg). Upon cooling, the dark green residue obtained was dissolved in CH_2Cl_2 (30 mL) and filtered, and the filtrate collected was vacuum distilled to remove solvent. The residue obtained was recrystallized from a CH_2Cl_2/hexane solvent mixture to give a green solid with a yield of about 70%. Mass spectral data [*m/z*, fragment]: 1289, $Ru_2(dpb)_4^+$; 1323, $Ru_2(dpb)_4Cl^+$. UV−vis (CH_2Cl_2, nm ($\varepsilon \times 10^{-3}$ L mol^{-1} cm^{-1})): 443 (4.7), 556 (1.5), 715 (2.9), 778 (3.0), 854 (1.0).

$Ru_2(dpb)_4(CO)$ (2). In a Schlenk flask, $Ru_2(dpb)_4Cl$ (0.050 g, 0.0378 mmol) was dissolved in CH_2Cl_2 (20 mL) and purged with nitrogen (2 min). Excess sodium borohydride was added to the CH_2Cl_2 solution and stirred until a color change from yellow green to red was observed. CO gas was then passed through the solution until it turned green (30 min), after which the solution was filtered. The

dx.doi.org/10.1021/ic5007605 | Inorg. Chem. 2014, 53, 7416−7428

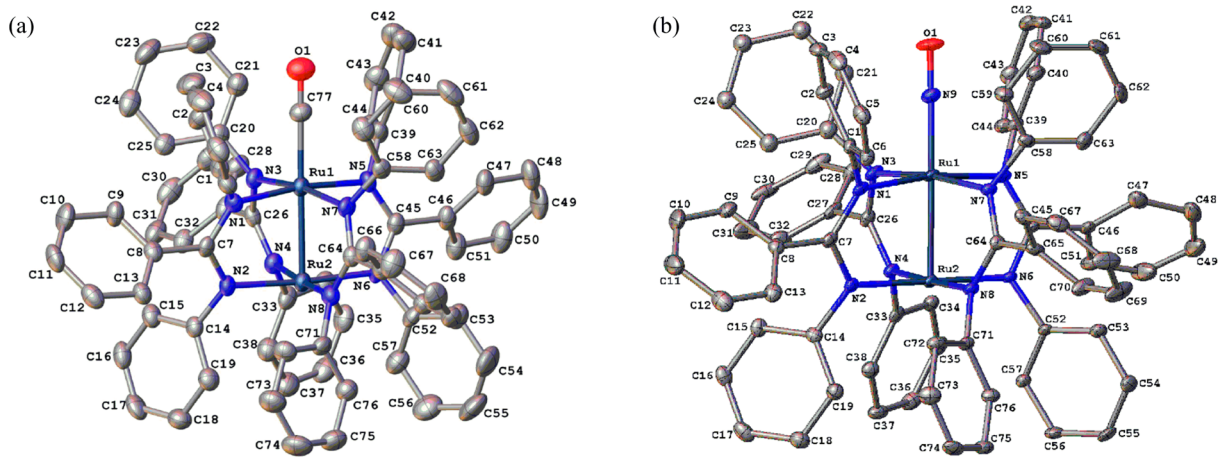

Figure 1. Molecular structures of (a) $Ru_2(dpb)_4(CO)$ **2-A** and (b) $Ru_2(dpb)_4(NO)$ **3**. The H atoms have been omitted for clarity.

filtrate was subsequently vacuum distilled to remove the solvent. The solid residue was recrystallized from a hexane/dichloromethane mixture to give a green solid (yield 90%). MS [*m*/*z*, fragment]: 1289, $Ru_2(dpb)_4^+$. UV–vis (CH_2Cl_2, nm ($\varepsilon \times 10^{-3}$ L mol^{-1} cm^{-1})): 411 (11.2), 472 (3.90), 586 (3.60), 703 (2.85). IR (KBr, cm^{-1}): 1924 (s) (ν_{co}), 2927 (m), 2854 (m), 1725 (w), 1594 (m), 1485 (s), 1285(s), 1272 (s), 1251(s), 1211 (w), 1114 (s), 1024 (w), 937 (w) and 900 (s).

$Ru_2(dpb)_4(NO)$ (3). In a Schlenk flask, $Ru_2(dpb)_4Cl$ (0.050 g, 0.0378 mmol) was dissolved in CH_2Cl_2 (20 mL) and purged with nitrogen (2 min). Nitric oxide (NO) gas was then passed through the solution until color of solution turned red (20 min). Nitrogen gas was used to purge out unreacted NO gas, and the color of the solution changed to green. The solution was then filtered, and the filtrate was subsequently vacuum distilled to remove the solvent. The solid residue was recrystallized from a hexane/dichloromethane mixture, and the solvents were decanted and the solids redissolved in dichloromethane (yield 90%). UV–vis (CH_2Cl_2, nm ($\varepsilon \times 10^{-3}$ L mol^{-1} cm^{-1})): 419 (5.5), 446 (5.0), 529 (4.0), 700 (8.9). MS [*m*/*z*, fragment]: 1289, $Ru_2(dpb)_4^+$. IR (KBr, cm^{-1}): 1778 (s) (ν_{NO}), 3666 (w), 3411 (br), 3066 (m), 1588 (m), 1486 (s), 1246 (s), 1207 (w), 1116 (s), 1071 (w), 1018 (m), 925 (s), 769 (m), 702 (s).

Single Crystal X-ray Diffraction Studies. Measurements were made with a Bruker SMART APEXII diffractometer equipped with a CCD area detector. The programs used in the X-ray diffraction studies were as follows: data collection, Apex2 (Bruker, 2009); cell refinement and data reduction, Bruker SAINT v7.12A (Bruker-Nonius, 2004); structure refinement and validation, SHELXTL (Sheldrick, 2008); and PLATON (Spek, 1990).

Green single crystals of **2** were obtained by slow evaporation of a CH_2Cl_2 solution. The unit cell contains one diruthenium complex (**2-A**, with atoms Ru1 and Ru2) in a general position, one diruthenium complex (**2-B** with atom Ru3) on the intersection of two 2-fold axes, one duruthenium complex (**2-C** with atoms Ru4) on a crystallographic 2-fold axis, and some diffusely diffracting solvent molecules that were not identified, *vide infra*.

The molecular structure of complex **2-A** is reliably established, and the complex was refined anisotropically. It is a problem-free part of the structure.

Complex **2-B** resides on the intersection of two 2-fold axes, and thus, only one-quarter of **2-B** is symmetry-independent. Strangely enough, this complex is present in the lattice only 81.4(2)% of the time. The C89 phenyl ring is disordered over two positions with the minor component being present 47.9(6)% of the time. The O2 carbonyl is equally disordered over two positions. This complex was refined with constraints and restraints.

Complex **2-C** resides on a crystallographic 2-fold axis. The Ru atom is disordered over two positions with the major component being present 64.4(3)% of the time. The other atoms exhibit large thermal displacement ellipsoids, but it was not possible to model the whole molecule disorder of the complex. Due to the disorder of atom Ru4 and unique position of the rest of the complex, some Ru–N and Ru–C distances are not chemically reasonable. This complex was refined with constraints and restraints. The phenyl ring C114 and the O3 carbonyl are equally disordered over two positions.

Additionally, there were several partially occupied solvent molecules present in the asymmetric unit. Bond length restraints were applied to model the molecules, but the resulting isotropic displacement coefficients suggested the molecules were mobile. In addition, the refinement was computationally unstable. Option SQUEEZE of the program PLATON was used to correct the diffraction data for diffuse scattering effects and to identify the solvent molecules. PLATON calculated the upper limit of volume that can be occupied by the solvent to be 4098 Å^3, or 16.8% of the unit cell volume. The program calculated 938 electrons in the unit cell for the diffuse species. It was not possible to confidently identify the solvent because compound **2** had been exposed to MeCN, CH_2Cl_2, EtOH, hexanes, and MeOH, meaning that any combination of these solvents could be present. The solvent molecules are disordered over several positions. It should be noted that all derived results in the following tables are based on the known contents. No data are given for the diffusely scattering species.

Dark sea green single crystals of **3**·*x*solvent were obtained by slow evaporation of a CH_2Cl_2 solution. There are also two molecules of dichloromethane solvent per Ru complex **3** in the lattice.

There is positional disorder in the structure. In the dinuclear complex, the phenyl ring at N3 is disordered over two positions in a 0.505(4):0.495(4) ratio. The disordered rings were refined isotropically with an idealized geometry. In one of the crystallization solvent dichloromethane molecules atoms Cl4 is disordered over two positions in a 0.852(5):0.148(5) ratio, and atoms Cl4 and Cl4a were refined with constraints.

There was an additional solvate molecule present in the asymmetric unit. Bond length restraints were applied to model the molecules, but the resulting isotropic displacement coefficients suggested that the molecules were mobile. In addition, the refinement was computationally unstable. Option SQUEEZE of the program PLATON was used to correct the diffraction data for diffuse scattering effects and to identify the solvate molecule. PLATON calculated the upper limit of volume that could be occupied by the solvent to be 559 Å^3, or 7.8% of the unit cell volume. The program calculated 58 electrons in the unit cell for the diffuse species. It is very likely that this solvate molecule is disordered over several positions. All derived results in the following tables are based on the known contents. No data are given for the diffusely scattering species.

dx.doi.org/10.1021/ic5007605 | *Inorg. Chem.* 2014, 53, 7416–7428

RESULTS AND DISCUSSION

Synthesis. $Ru_2(dpb)_4Cl$ (**1**) was synthesized by reaction of $Ru_2(OAc)_4Cl$ with molten dpb bridging ligand. Subsequent recrystallization in CH_2Cl_2 yielded the pure complex **1**.

The electrosynthesis of $Ru_2(dpf)_4(CO)$ under a CO atmosphere was first reported by Bear and Kadish,[38] and a few years later, the chemical synthesis of $[Ru_2(dpf)_3(OAc)(CO)]BF_4$ was reported by Barral et al.[33] In the present study, $Ru_2(dpb)_4(CO)$ (**2**) was prepared by reduction of $Ru_2(dpb)_4Cl$ using $NaBH_4$ and CH_2Cl_2 as solvent. CO gas was then passed through the solution to yield **2** which was purified by recrystallization in a hexane/acetone solvent mixture.

$Ru_2(dpb)_4(NO)$ (**3**) was synthesized by a chemical reaction of deaerated $Ru_2(dpb)_4Cl$ in CH_2Cl_2 saturated with nitric oxide; the excess NO was then removed by purging with nitrogen. Subsequent purification by recrystallization yielded pure samples of $Ru_2(dpb)_4(NO)$ (**3**).

The molecular structures of **2** and **3** are shown in Figure 1, whereas the crystallographic data are tabulated in Table 1 and selected metric parameters are listed in Table 2. All other structural data for **2** and **3** are given in the Supporting Information. In both complexes as well as in $Ru_2(dpf)_4(NO)$, atom Ru1 is in a distorted octahedral environment ligating to four N atoms in the equatorial plane, to the second Ru atom in one apical position and to a C or N atom in the other. The coordination environment of atom Ru2 is distorted octahedral with one vacant apical position, rendering this metal center five-coordinate. The Ru−Ru bond distances in **2** and **3** measure 2.4789(8) and 2.4119(5) Å. These bonds are shorter than the Ru−Ru bond distances in the corresponding dpf complexes. This trend is consistent with the fact that metal−metal bond distances in diruthenium complexes usually greatly depend on the type of equatorial ligands. The Ru−Ru bond lengths of all complexes in Table 2 are within the expected ranges of Ru−Ru bond distances in diruthenium complexes. In addition, the Ru−CO bond distances are appreciably longer than the Ru−NO bond lengths, and the change in $Ru-L_{ax}$ (L_{ax} = CO or NO) bond distance is larger for the dpf complex. The $Ru-Ru-L_{ax}$ bond angles of diruthenium complexes in Table 2 are all close to 180°. The bond angles are slightly different from each other for the dpb complexes with values of 178.4° or 178.5°, but are identical to each other for the dpf complexes with a value of 180°. All Ru−N distances are typical. In all three compounds atom Ru2 is displaced from the plane defined by the four-coordinated N atoms toward the CO or NO ligand by ∼0.15 Å whereas atom Ru2 is displaced in the opposite direction from its equatorial plane to a smaller extent (<0.07 Å). The coordination and geometry of the dpb ligand in **2** and **3**, and the dpf ligand in $Ru_2(dpf)_4(NO)$, are instructive to examine. The Ph rings on the N atom coordinated to Ru1 should form a much larger dihedral angle with the NCN chelating plane of the ligand than the Ph rings on the N atoms bonded to Ru2 in order to accommodate the carbonyl or nitrosyl ligands on one side of the complex and to compensate the absence of an apical ligand on the other. The respective angles for **2**, **3**, and $Ru_2(dpf)_4(NO)$ span 76(3)°, 75(3)°, and 78.1° at the Ru1 site and 68(5)°, 65(4)°, and 45.2° at the Ru2 end. The pairwise differences in the angle values in the same complexes are not statistically significant for **2**, probably statistically significant for **3**, and statistically significant for $Ru_2(dpf)_4(NO)$. Values closer to 90° are observed when the Ph ring must accommodate an additional ligand, and closer to 45° when the sixth ligand is absent. The magnitude of the angles may probably serve as indicators for the possible presence of carbonyl, nitrosyl, or monoatomic ligands in the case of positional disorder (and

Table 1. Crystal Data and Data Collection and Processing Parameters for Compounds 2 and 3

	$Ru_2(dpb)_4(CO)$ (**2**)	$Ru_2(dpb)_4(NO)$ (**3**)
mol formula	$C_{77}H_{60}N_8ORu_2$·unidentified solvent	$C_{78}H_{64}Cl_4N_9ORu_2$·unidentified solvent[a]
space group	$P\bar{4}c2$	$P2_1/n$
cell constant		
a (Å)	24.540(8)	13.9376(17)
b (Å)	24.540(8)	26.624(3)
c (Å)	40.500(13)	19.344(2)
α (deg)	90	90
β (deg)	90	91.940(2)
γ (deg)	90	90
V (Å^3)	24 389(14)	7 173.7(15)
Z	13.63	4
ρ_{calcd} (Mg/m^3)	1.221	1.377
μ (mm^{-1})	3.779	0.621
λ(Cu Kα) (Å)	1.54178	1.54178
T (K)	100(1)	100(1)
R (F_o)[b]	0.0457	0.0726
R_w (F_o)[c]	0.0414	0.0498

[a]With unidentified solvent. [b]$R = \sum||F_o| - |F_c||/\sum|F_o|$. [c]$R_w = [\sum_w(|F_o| - |F_c|)^2/\sum_w|F_o|^2]^{1/2}$.

Table 2. Selected Bond Length (Å) and Bond Angles (deg) of Compounds 2 and 3 along with Those of $Ru_2(dpf)_4(CO)$ and $Ru_2(dpf)_4(NO)$

	$Ru_2(dpb)_4(CO)$ (**2**)	$Ru_2(dpb)_4(NO)$ (**3**)	$Ru_2(dpf)_4(CO)$[c]	$Ru_2(dpf)_4(NO)$[d]
Ru−Ru	2.4789(8)	2.4119(5)	2.5544(8)	2.444(13)
$Ru1-N_L$[a]	2.074(14)[b]	2.08(2)	2.069(3)	2.065
$Ru2-N_L$[a]	2.027(8)[b]	2.017(19)[b]	2.028(3)	2.024
$Ru-L_{ax}$[a]	1.939(4)	1.824(4)	1.913(10)	1.809(11)
Y−O[a]	1.117(5)	1.166(5)	1.148(11)	1.142(12)
$Ru-Ru-L_{ax}$	179.35(12)	179.29(12)	180.00	180.00
Ru−Y−O	178.4(4)	178.5(4)	180.00	180.00
d(Ru1/N4)[b]	0.154(2)	0.1484(17)	0.177	0.166
d(Ru2/N4)[b]	−0.069(2)	−0.0144(16)	−0.068	−0.027

[a]Nitrogen of the bridging ligand (N_L), L = dpb or dpf. L_{ax} = axial ligand (CO or NO), Y = C or N. [b]Average values. d(Ru/N4)-displacement of the Ru atom from the plane defined by the 4 coordinated nitrogen atoms. [c]Reference 38. [d]Reference 39.

dx.doi.org/10.1021/ic5007605 | Inorg. Chem. 2014, 53, 7416−7428

partial occupancy) of these ligands. The idealized paddlewheel geometries of the complexes (C_{4v} or 4*mm* symmetry) are not observed because the chelating NCN planes of the dpb and dpf ligands are not coplanar with atoms Ru1 and Ru2. Thus, the paddlewheel assembly is replaced with a near C_4 (or 4 symmetry) propeller-like arrangement of the ligands about the Ru–Ru 4-fold axis. All ligands are tilted in the same direction relative to the Ru–Ru bond. The average N–Ru1–Ru2–N torsion angles in these three compounds are 13.9(5)°, 13.2(6)°, and 14.7°, illustrating consistent tilts of the "propeller blades".

UV–Vis Spectroscopy of $Ru_2(dpb)_4Cl$ in CH_2Cl_2 and PhCN. The UV–vis spectra of $Ru_2(dpb)_4Cl$ in neat CH_2Cl_2 and in CH_2Cl_2 solutions containing 0.1 M TBAX where X = ClO_4^-, Cl^-, or F^- are displayed in Figure 2.

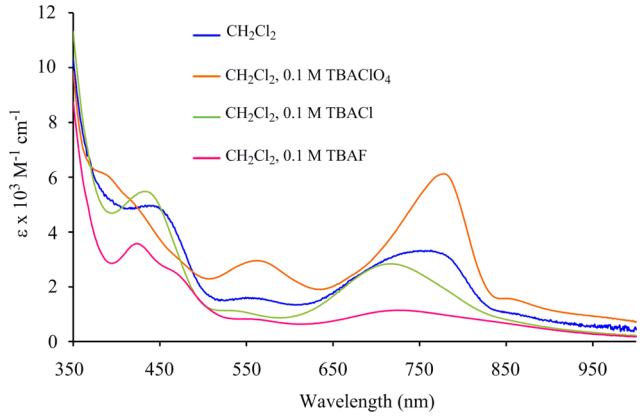

Figure 2. UV–vis spectra of $Ru_2(dpb)_4Cl$ (1.0×10^{-4} M) in neat CH_2Cl_2 and CH_2Cl_2 containing 0.1 M TBAX where X is ClO_4^-, Cl^-, and F^-.

The spectrum in neat CH_2Cl_2 exhibits a 778 nm band also seen in the solution containing 0.1 M $TBAClO_4$ and a 715 nm band that is seen in the solution containing 0.1 M TBACl. This suggests that the Ru_2^{5+} complex in neat CH_2Cl_2 exists as a mixture of two forms, $Ru_2(dpb)_4Cl$ and $[Ru_2(dpb)_4]^+$ (see eq 7), a result confirmed by monitoring the UV–vis spectra of $Ru_2(dpb)_4Cl$ at four different concentrations in CH_2Cl_2 where the cell path lengths were varied from 0.01 to 10 cm as the diruthenium concentration was decreased (see Supporting Information Figure S1).

$$Ru_2(dpb)_4Cl \rightleftarrows [Ru_2(dpb)_4]^+ + Cl^- \quad (7)$$

The spectrum in CH_2Cl_2 containing 0.1 M TBAF exhibits an absorption band at 470 nm, a spectral feature not found in the other UV–vis spectra depicted in Figure 2. Hence, the observation of a 470 nm band would suggest the presence of $Ru_2(dpb)_4F$ and/or possibly $[Ru_2(dpb)_4F_2]^-$ in solution. However, the 470 nm band is not seen in the UV–vis spectrum of $Ru_2(dpb)_4F$, a compound *in situ* generated by adding 1 equiv of F^- to a CH_2Cl_2 solution of $Ru_2(dpb)_4Cl$ (see Supporting Information Figure S2). Hence, this absorption band is most likely attributed to the bis-fluoride adduct $[Ru_2(dpb)_4F_2]^-$.

The UV–vis spectrum of $Ru_2(dpb)_4Cl$ in CH_2Cl_2 containing 0.1 M $TBAClO_4$ is virtually the same as the UV–vis spectrum of this compound with excess PF_6^-, I^-, or Br^- in CH_2Cl_2 (Supporting Information Figure S3), thus suggesting that all compounds exist in the cationic form $[Ru_2(dpb)_4]^+$ under the four solution conditions.

Figure 3 compares the UV–vis spectrum of $Ru_2(dpb)_4Cl$ in neat PhCN (—) with the spectrum in neat CH_2Cl_2 (---). In

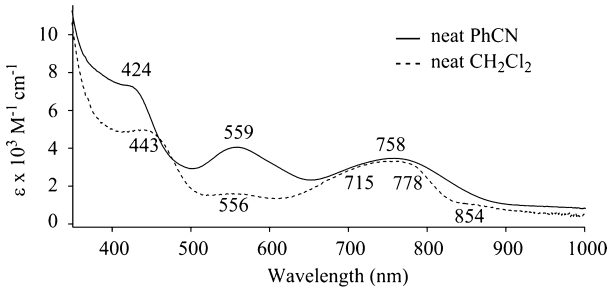

Figure 3. UV–vis spectra of $Ru_2(dpb)_4Cl$ (1.0×10^{-4} M) in neat CH_2Cl_2 and neat PhCN.

both solvents multiple bands are seen between 400 and 900 nm with the major differences being in the intensity and positions of the absorptions between 400 and 600 nm. These spectral differences suggest a possible coordination of PhCN to the diruthenium unit in PhCN, and this was confirmed by a spectrally monitored titration of $Ru_2(dpb)_4Cl$ in CH_2Cl_2 with PhCN (Figure 4a).

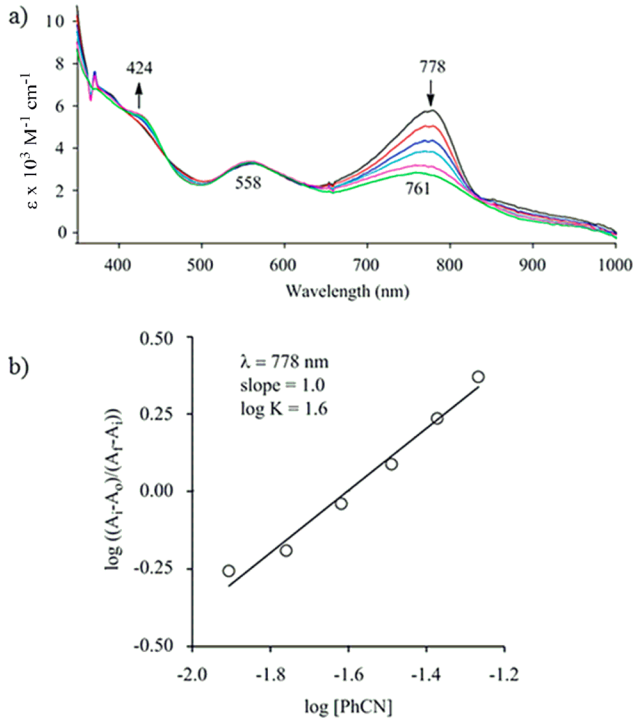

Figure 4. (a) Spectral changes during addition of PhCN to $Ru_2(dpb)_4Cl$ (1×10^{-4} M) in CH_2Cl_2 containing 0.1 M $TBAClO_4$ and (b) Hill plot analysis of the data.

The exact number of PhCN molecules bound to the Ru_2^{5+} species was ascertained using a Hill plot (Figure 4b). As shown in this figure, a linear relationship with a slope of 1.0 is obtained, hence suggesting the coordination of one and only one PhCN molecule to the diruthenium unit in its Ru_2^{5+} form. The PhCN bound compound is formulated as $[Ru_2(dpb)_4(PhCN)]^+$ in neat PhCN, and a log K = 1.6 was estimated for the ligand addition reaction (see eq 8) on the basis of the Hill plot.

dx.doi.org/10.1021/ic5007605 | *Inorg. Chem.* 2014, 53, 7416–7428

$$[Ru_2(dpb)_4]^+ + PhCN \rightleftarrows [Ru_2(dpb)_4(PhCN)]^+ \quad (8)$$

In addition, the UV−vis spectrum of $Ru_2(dpb)_4Cl$ in PhCN is virtually the same as the UV−vis spectrum of this compound in PhCN containing 0.1 M $TBAClO_4$ (Supporting Information Figure S4), therefore implying that the Ru_2^{5+} complex can be formulated as $[Ru_2(dpb)_4(PhCN)]^+$ under both solution conditions (with and without 0.1 M $TBAClO_4$ as supporting electrolyte).

In summary, the various forms of $Ru_2(dpb)_4Cl$ in CH_2Cl_2 containing 0.1 M TBAX when X = ClO_4^-, Cl^-, or F^- and in PhCN with or without $TBAClO_4$ are given in Scheme 1.

Scheme 1. Diruthenium Species Formed from $Ru_2(dpb)_4Cl$ in Solutions Containing Different Anions (X)

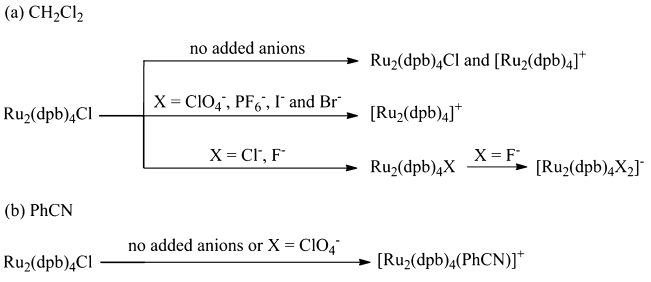

Electrochemistry in CH_2Cl_2. Cyclic voltammograms of $Ru_2(dpb)_4Cl$ in CH_2Cl_2 containing 0.1 M TBAX where X = ClO_4^-, Cl^-, or F^- are shown in Figure 5a−c. As depicted in Scheme 1, the major diruthenium form of $Ru_2(dpb)_4Cl$ in CH_2Cl_2, 0.1 M $TBAClO_4$, is assigned as $[Ru_2(dpb)_4]^+$ with a dissociated chloride ion. Under these solution conditions, the cyclic voltammogram exhibits two reduction processes on the cathodic (negative) scan which are labeled as I and II and two oxidation processes on the anodic (positive) scan which are labeled as III and IV (see Figure 5a). The first reversible reduction at $E_{1/2}$ = −0.26 V (process I) and the second irreversible reduction at E_{pc} = −1.80 V (process II) are assigned to the $Ru_2^{5+/4+}$ and $Ru_2^{4+/3+}$ processes of $[Ru_2(dpb)_4]^+$ on the basis of previously reported electrochemical behavior for numerous related $Ru_2(L)_4Cl$ complexes with a variety of different anionic bridging ligands, L.[18,34,40−42]

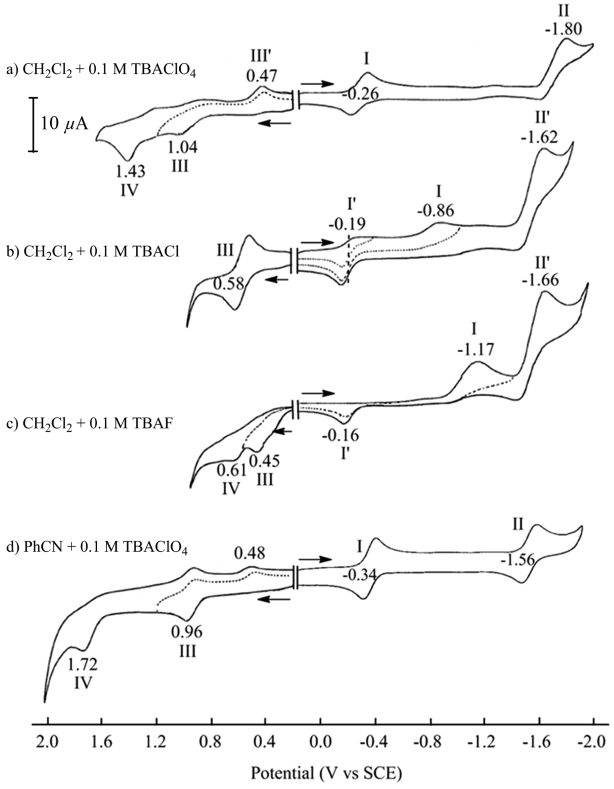

Figure 5. Cyclic voltammograms of $Ru_2(dpb)_4Cl$ in CH_2Cl_2 containing (a) 0.1 M $TBAClO_4$, (b) 0.1 M TBACl, and (c) 0.1 M TBAF or (d) in PhCN containing 0.1 M $TBAClO_4$.

The irreversible second reduction of $[Ru_2(dpb)_4]^+$ in CH_2Cl_2 has a much higher peak current than the first reduction at room temperature, but the two reductions at −70 °C are reversible and exhibit the same peak current height at $E_{1/2}$ = −0.27 and −1.64 V, respectively (see Supporting Information Figure S5). This is consistent with two stepwise one-electron additions. The difference between the electrochemical behavior at room temperature and that at low temperature is attributed to a chemical reaction involving the electrogenerated Ru_2^{3+} form of the compound and the CH_2Cl_2 solvent, as has been shown in the case of related Ru_2^{5+} complexes.[1]

The irreversible oxidation processes III and IV of $[Ru_2(dpb)_4]^+$ in Figure 5a are located at peak potentials of 1.04 and 1.43 V for a scan rate of 0.1 V/s. Process III is coupled with a reduction peak located at E_{pc} = 0.47 V (process III′) for a scan rate of 0.1 V/s. This process is assigned to reduction of a species that is not initially present in solution but is generated at the electrode surface, after the oxidation process III.

The most probable form of the electroactive species being re-reduced on the return scan at 0.47 V in Figure 5a is a chloride bound Ru_2^{6+} species, and we therefore propose the electrochemical EC mechanism shown in Scheme 2 to explain the oxidative behavior of $[Ru_2(dpb)_4]^+$. Since no major anodic (oxidation) process appears on positive potential sweeps prior to 1.04 V, process III is assigned to the initial oxidation of $[Ru_2(dpb)_4]^+$ in solution, which is the major form of the diruthenium compound in CH_2Cl_2 containing 0.1 M $TBAClO_4$ as indicated by the spectroscopic data (see Figure 2). The *in situ* generated one-electron oxidized dimetal compound, $[Ru_2(dpb)_4]^{2+}$, will undergo a rapid reaction with the free Cl^- ion present in solution (due to the initial dissociation of Cl^- from $Ru_2(dpb)_4Cl$) to yield $[Ru_2(dpb)_4Cl]^+$ which is then reduced on the return negative potential sweep to $Ru_2(dpb)_4Cl$ via process III′ at a peak potential of +0.47 V for a scan rate of 0.1 V/s.

Scheme 2. Overall Electron Transfer Mechanism for Oxidation of $Ru_2(dpb)_4Cl$ in CH_2Cl_2, 0.1 M $TBAClO_4$

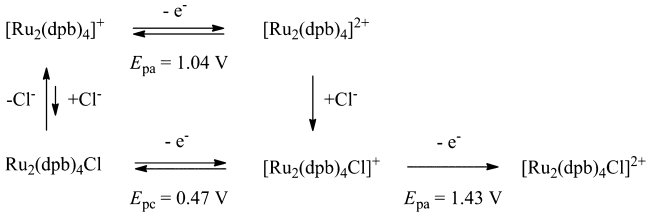

As shown in Scheme 2, the singly oxidized Ru_2^{6+} species formed after addition of Cl^- is formulated as $[Ru_2(dpb)_4Cl]^+$ and undergoes a one-electron oxidation at E_{pa} = 1.43 V for a scan rate of 0.1 V/s (process IV in Figure 5a). This reaction is 960 mV more positive than the potential for conversion of

dx.doi.org/10.1021/ic5007605 | Inorg. Chem. 2014, 53, 7416−7428

Scheme 3. Redox Reactions of $Ru_2(dpb)_4Cl$ in CH_2Cl_2, 0.1 M TBACl

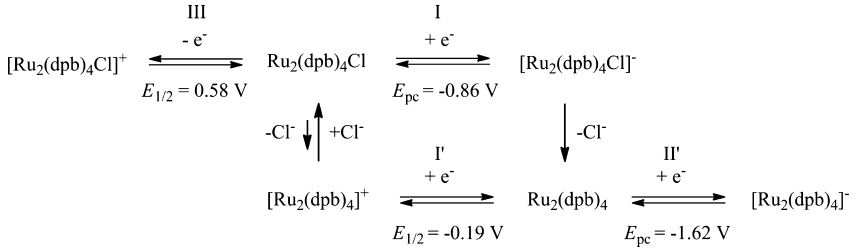

$[Ru_2(dpb)_4Cl]^+$ to $Ru_2(dpb)_4Cl$ (0.47 V), a result consistent with the observation that the potential gap between the reversible two oxidations of most $Ru_2(L)_4Cl$ complexes is usually close to 1.0 V.[17] Process IV is irreversible, thus suggesting that the electrogenerated Ru_2^{7+} species, $[Ru_2(dpb)_4Cl]^{2+}$, is unstable on the cyclic voltammetry time scale.[17,43]

As shown in Figure 5b,c, different redox behavior is seen when using TBACl or TBAF as supporting electrolyte. The major diruthenium species in solutions of 0.1 M TBACl is formulated as $Ru_2(dpb)_4Cl$. The cyclic voltammogram in this case exhibits three electrode processes labeled as I′, I, and II′ on the cathodic potential sweep whereas only one electrode process (process III) is seen on the anodic potential sweep (Figure 5b). Process I′ in Figure 5b occurs at a potential close to that for the peak assigned to process I in Figure 5a and thus is attributed to the one-electron reduction of $[Ru_2(dpb)_4]^+$. Process I, at −0.86 V, in Figure 5b has no corresponding peak in Figure 5a and is assigned to the one-electron reduction of the chloride bound Ru_2^{5+} compound $Ru_2(dpb)_4Cl$. It may appear odd that process I′ is assigned to a diruthenium species not initially present in solution. However, the potential difference between processes I′ and I in Figure 5b is fairly large (670 mV), and this would be the driving force for a dissociation of Cl^- from $Ru_2(dpb)_4Cl$ to give the more easily reducible $[Ru_2(dpb)_4]^+$ during the negative potential scan. A similar "potential driven" dissociation of Cl^- was shown to occur for $Ru_2(dpf)_4Cl$ during electroreduction in CH_2Cl_2 containing 0.1 M $TBAClO_4$.[43]

Process I is irreversible and coupled with process I′ on the return potential sweep, as shown by the dashed line in Figure 5b. This result suggests that the one-electron reduced form of $Ru_2(dpb)_4Cl$, i.e., $[Ru_2(dpb)_4Cl]^-$, undergoes a rapid dissociation of Cl^- on the cyclic voltammetry time scale to yield $Ru_2(dpb)_4$, which is then reoxidized via process I′ as shown in Scheme 3. As for the case of $Ru_2(dpb)_4Cl$ in CH_2Cl_2, 0.1 M $TBAClO_4$ (Figure 5a), the electrogenerated $Ru_2(dpb)_4$ complex present at the electrode surface after process I and loss of Cl^- undergoes an additional irreversible reduction at E_{pc} = −1.62 V to give $[Ru_2(dpb)_4]^-$ (process II′ for a scan rate of 0.1 V/s). Finally, the single well-defined oxidation at $E_{1/2}$ = 0.58 V (Figure 5b) is assigned to the reversible conversion of $Ru_2(dpb)_4Cl$ to $[Ru_2(dpb)_4Cl]^+$. Scheme 3 summarizes all of the electron transfer reactions involving $Ru_2(dpb)_4Cl$ in CH_2Cl_2, 0.1 M TBACl.

Fluoride ion will bind more strongly to Ru_2^{5+} than chloride ion, and this is reflected in the cyclic voltammogram of $Ru_2(dpb)_4Cl$ in CH_2Cl_2 containing 0.1 M TBAF as supporting electrolyte (Figure 5c). There are two reduction processes (labeled as I and II′) on the cathodic potential sweep from 0.0 to −2.0 V and two oxidations (labeled as III and IV) on the anodic potential sweep from 0.0 to +1.0 V. No electrode reaction assigned to $[Ru_2(dpb)_4]^+$ is observed on the initial sweep, thus suggesting that the fluoride ion remains tightly bound.

The spectroscopic data described earlier in the Article shows that the diruthenium complex exists as a mixture of $Ru_2(dpb)_4F$ and $[Ru_2(dpb)_4F_2]^-$ in CH_2Cl_2, 0.1 M TBAF (see Scheme 1,) and the first reduction peak I at −1.17 V in Figure 5c is therefore proposed to involve overlapping reduction processes of $Ru_2(dpb)_4F$ and $[Ru_2(dpb)_4F_2]^-$. These two diruthenium forms of the compound bear a different charge, i.e., 0 for $Ru_2(dpb)_4F$ and −1 for $[Ru_2(dpb)_4F_2]^-$, which would suggest a large difference in the reduction potentials between the mono- and bis-adducts. However, the fact that only one reduction is observed can be rationalized if $[Ru_2(dpb)_4F_2]^-$ is converted to $Ru_2(dpb)_4F$ prior to electron transfer. Alternatively, it may be that the second fluoride ion might bind more weakly to the diruthenium core as compared to the first fluoride ion, and thus, both reduction potentials might be similar to each other. Evidence for this possibility is given by the fact that only 1 equiv of F^- is needed to completely convert $Ru_2(dpb)_4Cl$ into $Ru_2(dpb)_4F$ (Supporting Information Figure S2), whereas about 1000 equiv of F^- must be added to solution in order to obtain $[Ru_2(dpb)_4F_2]^-$ (Figure 2).

The irreversible reduction process I in Figure 5c is located at E_{pc} = −1.17 V, and the compound formed at the electrode surface during this process is reoxidized via process I′ at E_{pa} = −0.16 V as shown by the dashed line on the return sweep. It should be noted that process I′ is not observed on the voltammogram in Figure 5c when the potential scan was reversed prior to process I (data not shown). The reoxidation process I′ in Figure 5b,c has virtually the same E_{pa} values which is not so different from the E_{pc} of process I in Figure 5a, and in all three cases these reactions correspond to the $Ru_2^{5+/4+}$ processes of $[Ru_2(dpb)_4]^+$. Therefore, one can propose that the reduced forms of $Ru_2(dpb)_4F$ and $[Ru_2(dpb)_4F_2]^-$ both undergo a rapid dissociation of the fluoride anion(s) to yield $Ru_2(dpb)_4$, which is then reoxidized via process I′ and further reduced via process II′.

As mentioned above, two electrode reactions are seen on the positive potential scan in Figure 5c. The first oxidation (process III) is attributed to the $Ru_2^{5+/6+}$ process of $[Ru_2(dpb)_4F_2]^-$, whereas the second oxidation (process IV) is attributed to the $Ru_2^{5+/6+}$ form of $Ru_2(dpb)_4F$. This assignment is based on the fact that $Ru_2(dpb)_4Cl$ in CH_2Cl_2, 0.1 M TBAF, exists as a mixture of $Ru_2(dpb)_4F$ and $[Ru_2(dpb)_4F_2]^-$ (as shown in Scheme 1) and that process IV occurs at a potential close to process III in Figure 5b, an electrode reaction attributed to the $Ru_2^{5+/6+}$ form of $Ru_2(dpb)_4Cl$.

Electrochemistry in PhCN. A cyclic voltammogram of $Ru_2(dpb)_4Cl$ in PhCN containing 0.1 M $TBAClO_4$ is shown in Figure 5d. On the basis of the UV−vis data discussed in a previous section of the Article, we proposed that $Ru_2(dpb)_4Cl$

dx.doi.org/10.1021/ic5007605 | Inorg. Chem. 2014, 53, 7416−7428

predominantly exists as $[Ru_2(dpb)_4PhCN)]^+$ under these solution conditions. As shown in Figure 5d, two major reductions (I and II) and two major oxidations (III and IV) are seen in the cyclic voltammogram of $Ru_2(dpb)_4Cl$ under these solution conditions. Processes I and II are both reversible on the cyclic voltammetry time scale. Process I is assigned to the $Ru_2^{5+/4+}$ reaction of $[Ru_2(dpb)_4(PhCN)]^+$ and would give as a reduction product $Ru_2(dpb)_4(PhCN)$, $Ru_2(dpb)_4(PhCN)_2$, or $Ru_2(dpb)_4$ depending upon the ability of PhCN to coordinate to the Ru_2^{4+} form of the compound. This point was elucidated by investigating the electrochemistry of $Ru_2(dpb)_4Cl$ in CH_2Cl_2/PhCN mixtures with different concentrations of PhCN and constructing plots of $E_{1/2}$ versus log[PhCN] for each redox process. These plots are shown in Figure 6 and can be divided into three regions as a function of log[PhCN].

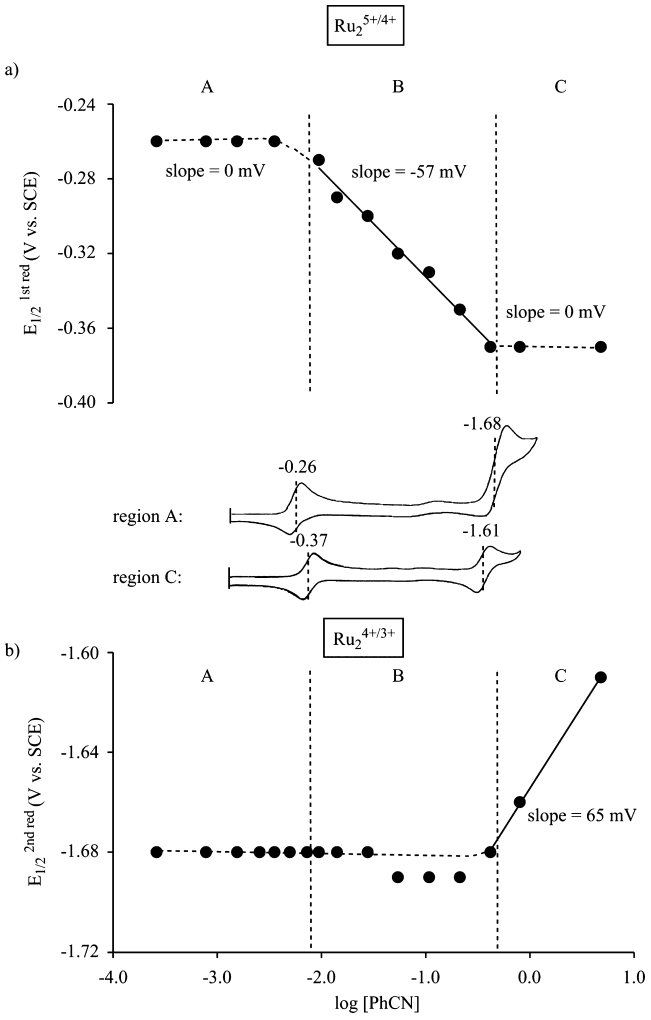

Figure 6. Plot of $E_{1/2}$ vs log[PhCN] of (a) $Ru_2^{5+/4+}$ and (b) $Ru_2^{4+/3+}$ processes upon addition of small aliquots of PhCN to a CH_2Cl_2, 0.1 M $TBAClO_4$, solution of $Ru_2(dpb)_4Cl$.

As the concentration of PhCN increases in the CH_2Cl_2/PhCN mixtures, $E_{1/2}$ of the $Ru_2^{5+/4+}$ process remains the same in region A or region C, but shifts toward more negative values with a slope of −57 mV in region B (Figure 6a). Likewise, an increase in PhCN concentration in the CH_2Cl_2/PhCN mixtures does not produce a large change in $E_{1/2}$ of the $Ru_2^{4+/3+}$ process in region A or region B, but yields a shift of $E_{1/2}$ toward more positive values with a slope of 65 mV in region C (see Figure 6b).

The electrode reactions shown in Scheme 4 can explain the features of the plots of $E_{1/2}$ versus log[PhCN] in Figure 6. In this scheme, the diruthenium complex is shown only by its core for simplicity. The $Ru_2(dpb)_4Cl$ complex exists as $[Ru_2(dpb)_4]^+$ in region A of low PhCN concentrations and is formulated as Ru_2^{5+} in Scheme 4, while the $Ru_2(dpb)_4Cl$ complex exists as $[Ru_2(dpb)_4(PhCN)]^+$ in regions B and C of higher PhCN concentrations and is formulated as $Ru_2^{5+}(PhCN)$ in Scheme 4. The PhCN molecule dissociates from the complex upon conversion of Ru_2^{5+} to Ru_2^{4+} in region B, but the solvent molecule remains coordinated after reduction in region C. This assignment is consistent with the fact that the plot of $E_{1/2}$ (1st red) versus log[PhCN] is linear with a slope of −57 mV in region B but has a $\Delta E_{1/2}/\Delta$ log[PhCN] value of 0 mV in region C. The $Ru_2^{4+/3+}$ process occurs without gain or loss of PhCN in both regions A and B whereas in region C (where the Ru_2^{4+} species predominantly exists as $Ru_2(dpb)_4(PhCN)$), one additional PhCN molecule binds to the Ru_2^{3+} product of the reaction, suggesting a formulation of $[Ru_2(dpb)_4(PhCN)_2]^-$ (shown as $Ru_2^{3+}(PhCN)_2$ in Scheme 4) in this region of PhCN concentration. This assignment of PhCN coordination is consistent with the fact that the plot of $E_{1/2}$ (2nd red.) versus log[PhCN] is linear with a slope of +65 mV in region C, while $E_{1/2}$ remains virtually invariant with change in PhCN concentration in both regions A and B.

Scheme 4. Overall Electron Transfer Mechanism of $Ru_2(dpb)_4Cl$ in CH_2Cl_2/PhCN, 0.1 M $TBAClO_4$, Mixtures with Regions A, B, and C Shown in Figure 6

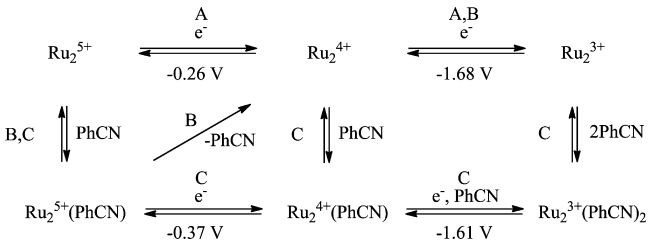

The data in Figure 6 were also used to evaluate the binding constants (K_1, K_2, and β_2) for the reactions illustrated by eqs 9−11 and were found to be approximately $10^{1.6}$, $10^{-0.06}$, and $10^{1.1}$, respectively.

$$[Ru_2^{5+}(dpb)_4]^+ + PhCN \rightleftarrows [Ru_2^{5+}(dpb)_4(PhCN)]^+ \quad \log K_1 = 1.6 \tag{9}$$

$$Ru_2^{4+}(dpb)_4 + PhCN \rightleftarrows Ru_2^{4+}(dpb)_4(PhCN) \quad \log K_2 = -0.06 \tag{10}$$

$$[Ru_2^{3+}(dpb)_4]^- + 2PhCN \rightleftarrows [Ru_2^{3+}(dpb)_4(PhCN)_2]^- \quad \log \beta_2 = 1.1 \tag{11}$$

UV−Vis Characterization of Electrogenerated Ru_2^{4+} and Ru_2^{6+}. The addition of one electron to $Ru_2(dpb)_4Cl$ can lead to four-, five-, or six-coordinate singly reduced Ru_2^{4+} products depending on the nature of added anions in solution as well as the solvent. For characterizing the Ru_2^{5+} reduction and oxidation products, the UV−vis spectral changes which occur during the $Ru_2^{5+/4+}$ and $Ru_2^{5+/6+}$ processes were

dx.doi.org/10.1021/ic5007605 | Inorg. Chem. 2014, 53, 7416−7428

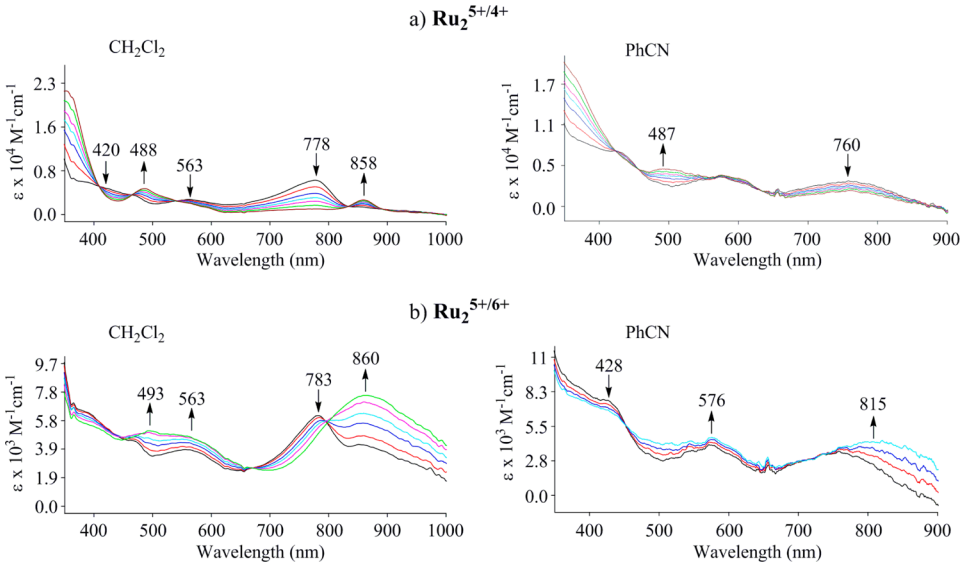

Figure 7. UV−vis spectral changes of $Ru_2(dpb)_4Cl$ during the (a) $Ru_2^{5+/4+}$ (E_{app} = −0.60 V) and (b) $Ru_2^{5+/6+}$ (E_{app} = 1.20 V) processes in CH_2Cl_2 and PhCN containing 0.1 M $TBAClO_4$.

monitored by thin-layer spectroelectrochemistry in CH_2Cl_2 and PhCN containing 0.1 M $TBAClO_4$, examples of which are shown in Figure 7. As seen in this figure, the absorption bands of $Ru_2(dpb)_4Cl$ in CH_2Cl_2, 0.1 M $TBAClO_4$, which are initially located at 420, 563, and 778 nm, decrease in intensity while new bands for the singly reduced Ru_2^{4+} grow in at 488 and 858 nm as the reaction proceeds (Figure 7a). Different spectral changes are seen in PhCN, 0.1 M $TBAClO_4$, where a new absorption band at 487 nm appears during the $Ru_2^{5+/4+}$ process and no new band at 858 nm is detected for the Ru_2^{4+} forms of $Ru_2(dpb)_4Cl$ under these solution conditions.

The products of the $Ru_2^{5+/4+}$ process are proposed to be $Ru_2(dpb)_4$ in CH_2Cl_2 and $Ru_2(dpb)_4(PhCN)$ in PhCN. The assignment of one bound solvent molecule to Ru_2^{4+} in PhCN is consistent with the electrochemical results obtained in CH_2Cl_2/PhCN mixtures (see Scheme 4).

The UV−vis spectral changes during the $Ru_2^{5+/6+}$ process of $Ru_2(dpb)_4Cl$ are also solvent dependent as illustrated in Figure 7b. In CH_2Cl_2, the Ru_2^{6+} species is characterized by bands at 493, 563, and 860 nm while two major bands at 576 and 815 nm are present in PhCN. The data in Figure 7b therefore suggests a different degree of solvent coordination for the Ru_2^{6+} form of the compound in PhCN and CH_2Cl_2, i.e., $[Ru_2(dpb)_4Cl]^+$ in CH_2Cl_2 and $[Ru_2(dpb)_4Cl(PhCN)]^+$ in PhCN. There are well-defined isosbestic points for the $Ru_2^{5+/6+}$ process in both solvents, thus indicating the absence of spectral intermediates during these electron transfer processes.

Electrochemistry of $Ru_2(dpb)_4(CO)$ and $Ru_2(dpb)_4Cl$ under CO. Cyclic voltammograms of $Ru_2(dpb)_4(CO)$ in CH_2Cl_2 containing 0.1 M $TBAClO_4$ under N_2 and under CO are shown in Figure 8a. Under both solution conditions, the compound exhibits a reversible one-electron reduction at ∼ −1.25 V and a reversible one-electron oxidation at 0.11 V vs SCE. Under N_2, there is also a reversible one-electron oxidation at 1.07 V and a reduction at −1.71 V which has much smaller peak current as compared to the other redox processes. Under a CO atmosphere the reduction at −1.71 V is not observed for $Ru_2(dpb)_4(CO)$ and the first oxidation at 1.07 V is followed by a second irreversible oxidation at E_{pa} = 1.34 V for a scan rate of 0.1 V/s.

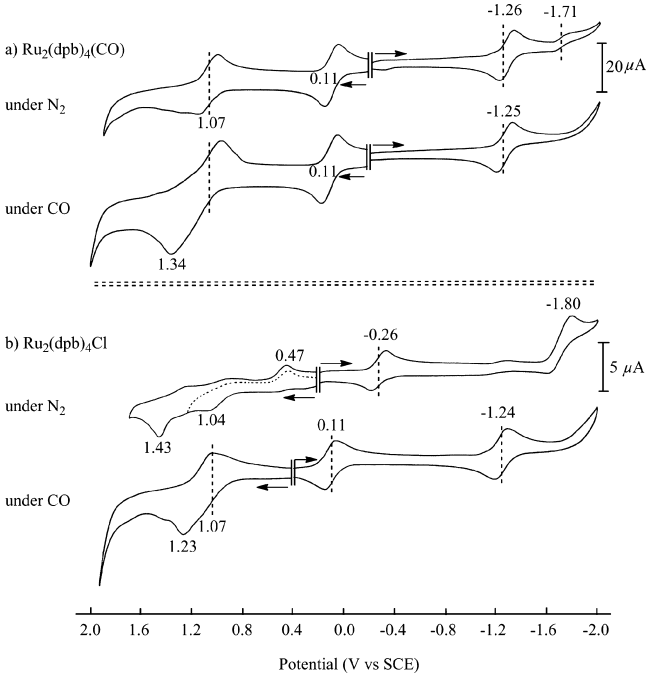

Figure 8. Cyclic voltammograms of (a) $Ru_2(dpb)_4(CO)$ and (b) $Ru_2(dpb)_4Cl$ in CH_2Cl_2 containing 0.1 M $TBAClO_4$ under a N_2 or CO atmosphere.

The effect of dissolved CO gas on the cyclic voltammograms of $Ru_2(dpb)_4(CO)$ in CH_2Cl_2, 0.1 M $TBAClO_4$ can be compared to the effect of this gas on the cyclic voltammograms of $Ru_2(dpf)_4(CO)$[38] under similar solution conditions. The latter compound was shown to exhibit a single reversible reduction at $E_{1/2}$ = −1.17 V under N_2 as compared to two reductions at −1.07 and −1.79 V under CO. There was also a single reversible oxidation at 0.28 V for $Ru_2(dpf)_4(CO)$[38] as compared to a reversible oxidation at 0.11 V for $Ru_2(dpb)_4(CO)$ under N_2 or CO (Figure 8a). Thus, $Ru_2(dpb)_4(CO)$ is easier to oxidize and harder to reduce than $Ru_2(dpf)_4(CO)$ under N_2 by 170 and 90 mV, respectively. In addition, $Ru_2(dpf)_4(CO)$ undergoes a second reduction

dx.doi.org/10.1021/ic5007605 | Inorg. Chem. 2014, 53, 7416−7428

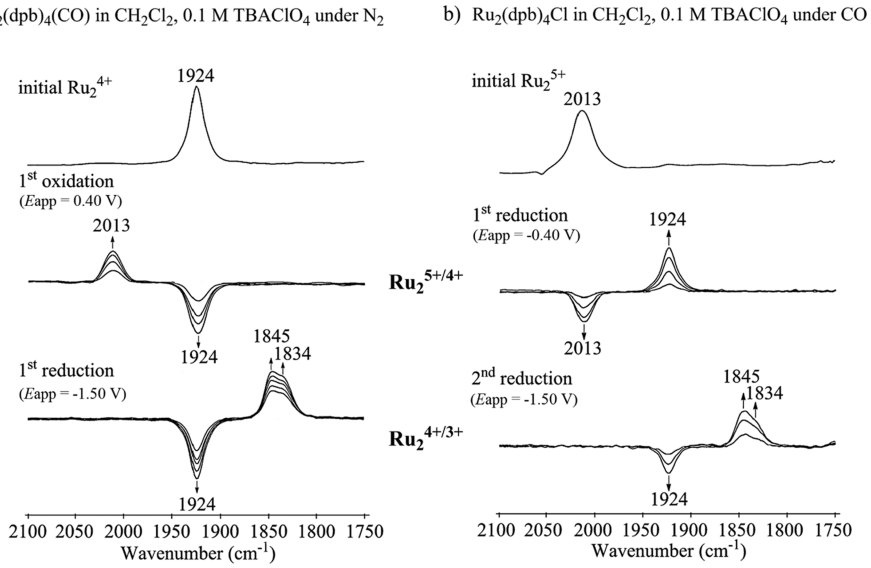

Figure 9. IR spectrum of (a) $Ru_2(dpb)_4(CO)$ under N_2 and (b) $Ru_2(dpb)_4Cl$ under CO in the absence of an applied potential (initial compounds) and during the first one-electron oxidation or reduction.

under CO that is not observed for $Ru_2(dpb)_4(CO)$ (see Figure 8a) under similar experimental conditions. The first reduction of $Ru_2(dpf)_4(CO)$ was assigned to the $Ru_2^{4+/3+}$ process while the first oxidation was attributed to $Ru_2^{4+/5+}$. A second one-electron oxidation of $Ru_2(dpb)_4(CO)$ is assigned to the $Ru_2^{5+/6+}$ electrode reaction. This process was not reported for $Ru_2(dpf)_4(CO)$ under CO.

The "minor" reduction process at −1.71 V in Figure 8a may involve an electrode reaction of the CO dissociated species, $Ru_2(dpb)_4$, based on the fact that the $Ru_2(dpb)_4/[Ru_2(dpb)_4]^-$ process of $Ru_2(dpb)_4Cl$ occurs at a similar potential (E_{pc} = −1.80 V) in CH_2Cl_2, 0.1 M $TBAClO_4$ (see top cyclic voltammogram in Figure 8b). This dissociation reaction would be slowed down under CO which would shift the equilibrium toward the CO bound species, and a redox process assigned to the unligated species would no longer be observed in the cyclic voltammogram at a scan rate of 0.1 V/s (see lower cyclic voltammogram in Figure 8a).

Evidence for the strong binding of a CO axial ligand to the Ru_2^{5+} form of $Ru_2(dpb)_4$ is shown in Figure 8b which compares cyclic voltammograms of $Ru_2(dpb)_4Cl$ under N_2 and after bubbling of CO gas through the solution. The conversion of $Ru_2(dpb)_4Cl$ to a CO bound species is rapid, and the cyclic voltammogram of the *"in situ"* generated product is virtually identical to that of the chemically generated and structurally characterized mono-CO diruthenium species in Figure 8a. Both compounds exhibit well-defined redox processes at 0.11 and ∼−1.25 V, and the main difference between the redox active species in Figure 8a and and that in Figure 8b under CO is that the *in situ* generated CO containing species exists in a Ru_2^{5+} oxidation state and is also associated with a Cl^- counteranion. Evidence for this assignment is given by the IR spectroelectrochemical results described in the following sections.

IR Spectroelectrochemistry of $Ru_2(dpb)_4(CO)$ and $Ru_2(dpb)_4Cl$ under CO. The same two compounds in Figure 8 were investigated under a CO atmosphere by thin-layer IR spectroelectrochemistry in order to characterize the CO vibration of the neutral compounds as well as the reduced and oxidized forms of the diruthenium species under the application of an applied potential. The use of thin-layer IR spectroelectrochemistry to monitor CO adducts of diruthenium compounds is described in earlier publications.[38,39,41,44]

The infrared spectrum for the Ru_2^{4+} complex $Ru_2(dpb)_4(CO)$ in CH_2Cl_2, 0.1 M $TBAClO_4$, is characterized by a CO stretching vibration band at ν_{CO} = 1924 cm^{-1}, while that of the electrochemically generated Ru_2^{5+} and Ru_2^{3+} species exhibit ν_{CO} vibrations at 2013 and 1845/1834 cm^{-1}, respectively, as shown in Figure 9a. The oxidized form of $Ru_2(dpb)_4(CO)$ under N_2 may be formulated as $[Ru_2(dpb)_4(CO)]^+$. The reduced form of $Ru_2(dpb)_4(CO)$ under N_2 exists as a mixture of mono- and bis-CO adducts that are, respectively, formulated as $[Ru_2(dpb)_4(CO)]^-$ and $[Ru_2(dpb)_4(CO)_2]^-$. The former compound is proposed to have a CO stretching vibration at 1834 cm^{-1} whereas the latter compound is proposed to have a CO stretching vibration at 1845 cm^{-1}. The presence of two forms of CO adducts for the Ru_2^{3+} forms of the compound and their CO stretching vibration assignment is based on the fact that, under a CO atmosphere, the Ru_2^{3+} species is characterized by only one CO stretching vibration at 1845 cm^{-1} (see Supporting Information Figure S6). Indeed, under these latter experimental conditions, only the bis-CO adduct, namely $[Ru_2(dpb)_4(CO)_2]^-$, would be expected to be formed during the Ru_2^{4+}/Ru_2^{3+} process of $Ru_2(dpb)_4(CO)$ under a CO atmosphere. As shown in Scheme 5, under N_2, the bis-CO adduct $[Ru_2(dpb)_4(CO)_2]^-$ is proposed to be obtained via a reaction between singly reduced $[Ru_2(dpb)_4(CO)]^-$ and CO gas released during dissociation from the initial complex as described in Figure 8a. This then yields $[Ru_2(dpb)_4(CO)_2]^-$ (ν_{co} = 1845 cm^{-1}) in addition to the original Ru_2^{3+} complex, $[Ru_2(dpb)_4(CO)]^-$ (ν_{co} = 1834 cm^{-1}), thus giving two IR bands in the spectrum of the singly reduced species. The shifts

Scheme 5. Reductions of $Ru_2(dpb)_4(CO)$ under N_2

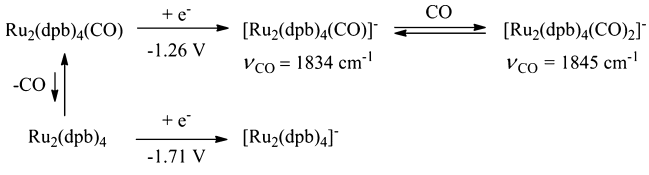

dx.doi.org/10.1021/ic5007605 | Inorg. Chem. 2014, 53, 7416−7428

in the CO stretching vibration upon going from $Ru_2(dpb)_4(CO)$ to $[Ru_2(dpb)_4(CO)]^+$ or $Ru_2(dpb)_4(CO)$ to $[Ru_2(dpb)_4(CO)]^-/[Ru_2(dpb)_4(CO)_2]^-$ are similar to shifts in ν_{CO} seen after the one-electron oxidation and one-electron reduction of $Ru_2(dpf)_4(CO)$ in CH_2Cl_2 under N_2.[38]

Figure 9b illustrates the measured CO stretching frequencies of the neutral and singly reduced forms of $Ru_2(dpb)_4Cl$ in CH_2Cl_2 containing 0.1 M $TBAClO_4$ after bubbling CO through the solution. There are no characteristic CO stretching vibrations for $Ru_2(dpb)_4Cl$ under N_2, but after replacing N_2 by CO, the $Ru_2(dpb)_4Cl$ in solution is converted to a species which exhibits a single CO stretch at 2013 cm^{-1} (Figure 9b), thus suggesting the coordination of one CO molecule to the Ru_2^{5+} form of the compound.

The 2013 cm^{-1} band for $Ru_2(dpb)_4Cl$ under CO is at exactly the same position as the ν_{CO} vibration of singly oxidized $Ru_2(dpb)_4(CO)$ in CH_2Cl_2 (Figure 9a). As discussed in an earlier section of the Article, $Ru_2(dpb)_4Cl$ dissociates to give $[Ru_2(dpb)_4]^+$ and Cl^- in CH_2Cl_2 containing 0.1 M $TBAClO_4$ under N_2, and the product of CO binding under a CO atmosphere is therefore proposed to be $[Ru_2(dpb)_4(CO)]^+$.

The first reduction of $Ru_2(dpb)_4Cl$ under CO occurs at $E_{1/2}$ = +0.11 V (Figure 8b), and under the application of an applied reduction potential, the ν_{CO} band at 2013 cm^{-1} disappears and is replaced by a strong ν_{CO} band at 1924 cm^{-1} (middle spectrum in Figure 9b). The same value of ν_{CO} is seen for the Ru_2^{4+} form of structurally characterized $Ru_2(dpb)_4(CO)$ (top spectrum in Figure 9a). Finally, the reduction of $Ru_2(dpb)_4(CO)$ under N_2 (Figure 9a) or $Ru_2(dpb)_4Cl$ under CO (Figure 9b) at an applied potential of −1.50 V in the thin-layer IR cell leads to an almost identical IR spectrum for the Ru_2^{3+} species, which is characterized by ν_{CO} bands at 1845 and 1834 cm^{-1}.

We have shown in an earlier section of the Article that $Ru_2(dpb)_4Cl$ exists in CH_2Cl_2 (with no $TBAClO_4$ added) as a mixture of $[Ru_2(dpb)_4]^+$ and $Ru_2(dpb)_4Cl$, where the proportion of the two forms of the compound is concentration dependent. The IR spectrum of $Ru_2(dpb)_4Cl$ under a CO atmosphere in CH_2Cl_2 without any added $TBAClO_4$ is shown in Figure 10a and exhibits two CO stretching bands, a major band at 2013 and a less intense band at 1993 cm^{-1} which appears as a shoulder. This suggests the presence of two Ru_2^{5+} CO adducts in solution. The band at 2013 cm^{-1} is assigned to the ν_{CO} of $[Ru_2(dpb)_4(CO)]^+$ while the band at 1993 cm^{-1} is most likely due to $Ru_2(dpb)_4Cl(CO)$. As shown in Scheme 1, only $[Ru_2(dpb)_4]^+$ exists in a CH_2Cl_2, 0.1 M $TBAClO_4$, solution, and under these solution conditions only $[Ru_2(dpb)_4(CO)]^+$ should be present in solution under a CO atmosphere. This is indeed the case as shown in Figure 10b. $Ru_2(dpb)_4Cl(CO)$ would be expected to have a higher electron density on the Ru_2^{5+} dimetal unit than does $[Ru_2(dpb)_4(CO)]^+$, because of the axially bound Cl^- anion.

Interestingly, the present work shows that CO reacts with $Ru_2(dpb)_4Cl$, a result that differs from what has previously been reported for other ap or substituted ap derivatives.[41] It also differs from $Ru_2(dpf)_3(OAc)Cl$,[33] which showed no evidence for the CO binding to the compound in its Ru_2^{5+} oxidation state. The lack of reactivity between CO and $Ru_2(dpf)_3(OAc)Cl$ was explained by the fact that the chloride anion inhibited the axial binding of CO to the dimetal unit.

Electrochemistry and IR Spectroelectrochemistry of $Ru_2(dpb)_4(NO)$. $Ru_2(dpb)_4(NO)$ in CH_2Cl_2, 0.1 M $TBAClO_4$, exhibits two one-electron reversible reductions and a single one-electron reversible oxidation (see Figure 11a).The reductions are located at $E_{1/2}$ = −0.04 and −1.52 V while the oxidation is seen at $E_{1/2}$ = 1.46 V. A related Ru_2^{3+} derivative, $Ru_2(dpf)_4(NO)$,[39] was previously characterized by two reversible reductions at $E_{1/2}$ = 0.06 and −1.24 V, but no oxidations were reported. Both reductions of $Ru_2(dpf)_4(NO)$ were assigned to metal-centered processes generating diruthe-

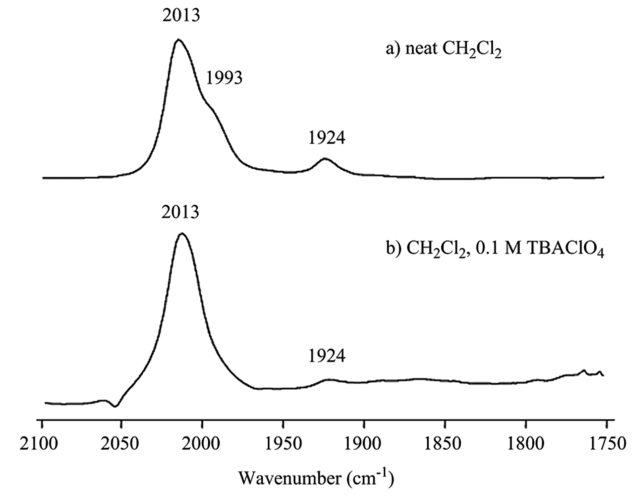

Figure 10. IR spectra of $Ru_2(dpb)_4Cl$ under a CO atmosphere in (a) neat CH_2Cl_2 and (b) CH_2Cl_2, 0.1 M $TBAClO_4$.

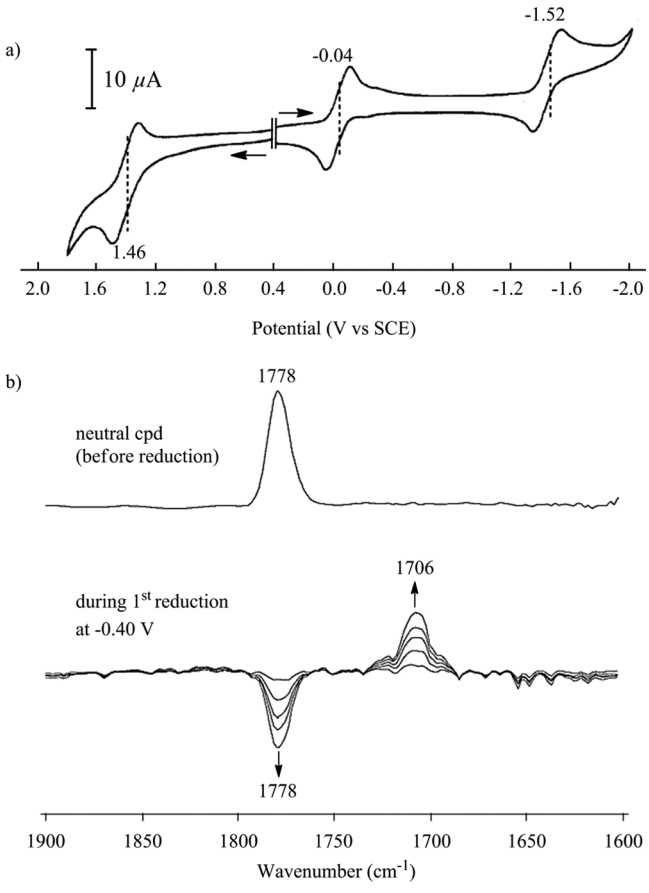

Figure 11. (a) Cyclic voltammogram in CH_2Cl_2, 0.1 M $TBAClO_4$, and (b) IR spectrum of $Ru_2(dpb)_4(NO)$ in the same solution before and after controlled potential reduction by one electron at −0.40 V.

dx.doi.org/10.1021/ic5007605 | Inorg. Chem. 2014, 53, 7416−7428

Table 3. Summary of Electrochemical and IR Spectral Data of Diruthenium Complexes

compd	formal oxidn state	axial ligand	stretching frequency, cm^{-1}		$E_{1/2}$ (V vs SCE)[a]					ref
			ν_{CO}	ν_{NO}	$Ru_2^{6+/5+}$	$Ru_2^{5+/4+}$	$Ru_2^{4+/3+}$	$Ru_2^{3+/2+}$	$Ru_2^{2+/1+}$	
$Ru_2(dpb)_4Cl$	Ru_2^{5+}	Cl^-	1993[b]		0.58	−0.19	−1.62[c]			tw
$[Ru_2(dpb)_4]^+$	Ru_2^{5+}		2013[b]		1.04[c]	−0.26	−1.80[c]			tw
$[Ru_2(dpb)_4(PhCN)]^+$	Ru_2^{5+}	PhCN			0.96[c,d]	−0.34[d]	−1.56[d]			tw
$[Ru_2(dpb)_4(CO)]^+$	Ru_2^{5+}	CO	2013							tw
$Ru_2(dpb)_4(CO)$	Ru_2^{4+}	CO	1924		1.07	0.11	−1.26			tw
$[Ru_2(dpb)_4(CO)]^-$	Ru_2^{3+}	CO	1834, 1845							tw
$Ru_2(dpb)_4(NO)$	Ru_2^{3+}	NO		1778			1.46	−0.04	−1.52	tw
$[Ru_2(dpb)_4(NO)]^-$	Ru_2^{2+}	NO		1706						tw
$Ru_2(dpf)_4Cl$	Ru_2^{5+}	Cl^-			0.54	−0.64[c]				43
$[Ru_2(dpf)_4(CO)]^+$	Ru_2^{5+}	CO	2019							38
$Ru_2(dpf)_4(CO)$	Ru_2^{4+}	CO	1929			0.28	−1.17			38
$[Ru_2(dpf)_4(CO)]^-$	Ru_2^{3+}	CO	1840							38
$Ru_2(dpf)_4(NO)$	Ru_2^{3+}	NO		1786				0.06	−1.24	39
$[Ru_2(dpf)_4(NO)]^-$	Ru_2^{2+}	NO		1712						39

[a]In CH_2Cl_2, 0.1 M TBAP. [b]In CH_2Cl_2 under CO. [c]Peak potential at the scan rate of 0.1 V/s. [d]In PhCN, 0.1 M TBAP; tw = this work.

nium complexes with formal oxidation states of Ru_2^{2+} and Ru_2^{1+}, respectively, and the same assignment is given in the case of $Ru_2(dpb)_4(NO)$. The currently investigated dpb NO derivative is more difficult to reduce by 100−280 mV, consistent with the stronger donor character of the dpb ligand.

The neutral and singly reduced forms of $Ru_2(dpb)_4(NO)$ were characterized by thin-layer IR spectroelectrochemistry, an example of which is shown in Figure 11b. The infrared spectrum of neutral $Ru_2(dpb)_4(NO)$ in CH_2Cl_2 containing 0.1 M $TBAClO_4$ exhibits an ν_{NO} at 1778 cm^{-1}. This value is close to the measured ν_{NO} of $Ru_2(dpf)_4(NO)$ at 1786 cm^{-1} and $[Ru_2(dpf)_4(NO)_2]^+$ at 1788 cm^{-1}, both of which are examples of Ru_2^{3+} complexes.[39] This 8−10 cm^{-1} difference in ν_{NO} between the dpb and dpf derivatives can be accounted for by an increased electron density on the dimetal unit in $Ru_2(dpb)_4(NO)$ which would lead to a stronger π back-donation to the antibonding π^* orbital of the NO axial ligand, thus causing the NO vibration band to shift to a lower frequency. As shown in Figure 11b, the ν_{NO} value of $Ru_2(dpb)_4(NO)$ at 1778 cm^{-1} shifts to 1706 cm^{-1} upon addition of one electron. This 72 cm^{-1} shift in the NO stretching vibration is comparable to the 71−74 cm^{-1} shifts reported for the one-electron reduction of $Ru_2(dpf)_4(NO)$ or $Ru_2(Fap)_4(NO)Cl$. A summary of electrochemical and IR spectral data of the dpb diruthenium complexes along with data for the dpf diruthenium complexes is given in Table 3.

SUMMARY

Three diruthenium complexes were synthesized with Cl, CO, or NO axial ligands and are characterized as to their electrochemical and spectroscopic properties. The reversibility and the potentials at which the electron transfer processes occur depend on both the solvent and the bound axial ligand, thus showing how a simple change in axial ligation can significantly affect the redox properties of diruthenium compounds with the same set of four bridging ligands. In addition, $Ru_2(dpb)_4Cl$ undergoes a facile conversion to $[Ru_2(dpb)_4(CO)]^+$ by simply bubbling CO gas through a CH_2Cl_2 solution of the diruthenium compound. $Ru_2(dpb)_4(NO)$ undergoes a reversible Ru_2^{3+}/Ru_2^{4+} redox process which has not been reported in the case of the related dpf complex, but is known in the case of $Ru_2(Fap)_4(NO)Cl$. Overall, the electron transfer processes of the dpb complexes occur at more negative potentials than those of the related dpf complexes, a result which is attributed to an increased electron density on the dimetal unit brought about by a higher basicity of the dpb ligand.

ASSOCIATED CONTENT

Supporting Information

Neutral UV−vis spectra and cyclic voltammograms of $Ru_2(dpb)_4Cl$ and IR spectral changes of $Ru_2(dpb)_4(CO)$ during the applied potential. Crystallographic data in CIF format. This material is available free of charge via the Internet at http://pubs.acs.org.

AUTHOR INFORMATION

Corresponding Authors

*E-mail: hanb@uww.edu.
*E-mail: kkadish@uh.edu.

Notes

The authors declare no competing financial interest.

ACKNOWLEDGMENTS

We gratefully acknowledge support from the Robert A. Welch Foundation (K.M.K., Grants E-680 and A0-0001) and the Teaching Reassignment Program in the College of Letters and Sciences at the UW—Whitewater (B.H.).

REFERENCES

(1) Ngubane, S.; Kadish, K. M.; Bear, J. L.; Van Caemelbecke, E.; Thuriere, A.; Ramirez, K. P. *Dalton Trans.* **2013**, *42*, 3571−3580.
(2) Cummings, S. P.; Savchenko, J.; Fanwick, P. E.; Kharlamova, A.; Ren, T. *Organometallics* **2013**, *32*, 1129−1132.
(3) Villalobos, L.; Cao, Z.; Fanwick, P. E.; Ren, T. *J. Chem. Soc., Dalton Trans.* **2012**, *41*, 644−650.
(4) Santos, R. L. S. R.; van Eldik, R.; de Oliveira Silva, D. *Inorg. Chem.* **2012**, *51*, 6615−6625.
(5) Delgado, P.; Gonzalez-Prieto, R.; Jimenez-Aparicio, R.; Perles, J.; Priego, J. L.; Torres, R. M. *Dalton Trans.* **2012**, *41*, 11866−11874.

(6) Boyd, D. A.; Cao, Z.; Song, Y.; Wang, T.-W.; Fanwick, P. E.; Crutchley, R. J.; Ren, T. *Inorg. Chem.* **2010**, *49*, 11525−11531.
(7) Fan, Y.; Fanwick, P. E.; Ren, T. *Polyhedron* **2009**, *28*, 3654−3658.
(8) Kadish, K. M.; Garcia, R.; Phan, T.; Wellhoff, J.; Van Caemelbecke, E.; Bear, J. L. *Inorg. Chem.* **2008**, *47*, 11423−11428.
(9) Castro, M. A.; Roitberg, A. E.; Cukiernik, F. D. *Inorg. Chem.* **2008**, *47*, 4682−4690.
(10) Kaim, W.; Sarkar, B. *Coord. Chem. Rev.* **2007**, *251*, 584−594.
(11) Barral, M. C.; Gallo, T.; Herrero, S.; Jiménez-Aparicio, R.; Torres, M. R.; Urbanos, F. *Chem.—Eur. J.* **2007**, *13*, 10088−10095.
(12) Barral, M. C.; Gonzalez-Prieto, R.; Jimenez-Aparicio, R.; Priego, J. L.; Torres, M. R.; Urbanos, F. A. *Eur. J. Inorg. Chem.* **2006**, 4229−4232.
(13) Barral, M. C.; Herrero, S.; Jiménez-Aparicio, R.; Torres, M. R.; Urbanos, F. A. *Angew. Chem., Int. Ed.* **2005**, *44*, 305−307.
(14) Angaridis, P. In *Multiple Bonds Between Metal Atoms*, 3rd ed.; Cotton, F. A., Murillo, C. A., Walton, R. A., Eds.; Springer Science and Business Media Inc.: New York, 2005.
(15) Aquino, M. A. S. *Coord. Chem. Rev.* **2004**, *248*, 1025−1045.
(16) Miyasaka, H.; Izawa, T.; Sugiura, K.; Yamashita, M. *Inorg. Chem.* **2003**, *42*, 7683−7690.
(17) Kadish, K. M.; Wang, L.-L.; Thuriere, A.; Van Caemelbecke, E.; Bear, J. L. *Inorg. Chem.* **2003**, *42*, 834−843.
(18) Kachi-Terajima, C.; Miyasaka, H.; Ishii, T.; Sugiura, K.-i.; Yamashita, M. *Inorg. Chim. Acta* **2002**, *332*, 210−215.
(19) Campos-Fernández, C. S.; Ouyang, X.; Dunbar, K. R. *Inorg. Chem.* **2000**, *39*, 2432−2433.
(20) Ren, T. *Coord. Chem. Rev.* **1998**, *175*, 43−58.
(21) Cotton, F. A.; Yokochi, A. *Inorg. Chem.* **1998**, *37*, 2723−2728.
(22) Aquino, M. A. S. *Coord. Chem. Rev.* **1998**, *170*, 141−202.
(23) Bear, J. L.; Li, Y.; Han, B.; Van Caemelbecke, E.; Kadish, K. M. *Inorg. Chem.* **1997**, *36*, 5449−5456.
(24) McCarthy, H. J.; Tocher, D. A. *Inorg. Chim. Acta* **1989**, *158*, 1−2.
(25) Chakravarty, A. R.; Cotton, F. A. *Inorg. Chim. Acta* **1986**, *113*, 19−26.
(26) Chakravarty, A. R.; Cotton, F. A.; Tocher, D. A. *Inorg. Chem.* **1985**, *24*, 2857−2861.
(27) Malinski, T.; Chang, D.; Feldmann, F. N.; Bear, J. L.; Kadish, K. M. *Inorg. Chem.* **1983**, *22*, 3225−3233.
(28) Stephenson, T. A.; Wilkinson, G. *J. Inorg. Nucl. Chem.* **1966**, *28*, 2285−2291.
(29) Campos-Fernández, C. S.; Thomson, L. M.; Galán-Mascarós, J. R.; Ouyang, X.; Dunbar, K. R. *Inorg. Chem.* **2002**, *41*, 1523−1533.
(30) McCarthy, H. J.; Tocher, D. A. *Polyhedron* **1992**, *11*, 13−20.
(31) Bear, J. L.; Chen, W.-Z.; Han, B.; Huang, S.; Wang, L.-L.; Thuriere, A.; Van Caemelbecke, E.; Kadish, K. M.; Ren, T. *Inorg. Chem.* **2003**, *42*, 6230−6240.
(32) Barral, M. C.; Gallo, T.; Herrero, S.; Jiménez-Aparicio, R.; Torres, M. R.; Urbanos, F. A. *Inorg. Chem.* **2006**, *45*, 3639−3647.
(33) Barral, M. C.; Herrero, S.; Jiménez-Aparicio, R.; Torres, M. R.; Urbanos, F. A. *J. Organomet. Chem.* **2008**, *693*, 1597−1604.
(34) Kadish, K. M.; Nguyen, M.; Van Caemelbecke, E.; Bear, J. L. *Inorg. Chem.* **2006**, *45*, 5996−6003.
(35) Lin, X. Q.; Kadish, K. M. *Anal. Chem.* **1985**, *57*, 1498−1501.
(36) Ellis, P. E., Jr.; Linard, J. E.; Szymanski, T.; Jones, R. D.; Budge, J. R.; Basolo, F. *J. Am. Chem. Soc.* **1980**, *102*, 1889−96.
(37) He, L. P.; Yao, C. L.; Naris, M.; Lee, J. C.; Korp, J. D.; Bear, J. L. *Inorg. Chem.* **1992**, *31*, 620−625.
(38) Kadish, K. M.; Han, B.; Shao, J.; Ou, Z.; Bear, J. L. *Inorg. Chem.* **2001**, *40*, 6848−6851.
(39) Han, B.; Shao, J.; Ou, Z.; Phan, T. D.; Shen, J.; Bear, J. L.; Kadish, K. M. *Inorg. Chem.* **2004**, *43*, 7741−7751.
(40) Chen, W.-Z.; Protasiewicz, J. D.; Davis, S. A.; Updegraff, J. B.; Ma, L.-Q.; Fanwick, P. E.; Ren, T. *Inorg. Chem.* **2007**, *46*, 3775−3782.
(41) Kadish, K. M.; Phan, T. D.; Giribabu, L.; Shao, J.; Wang, L.-L.; Thuriere, A.; Van Caemelbecke, E.; Bear, J. L. *Inorg. Chem.* **2004**, *43*, 1012−1020.
(42) Kadish, K. M.; Wang, L.-L.; Thuriere, A.; Giribabu, L.; Garcia, R.; Van Caemelbecke, E.; Bear, J. L. *Inorg. Chem.* **2003**, *42*, 8309−8319.
(43) Bear, J. L.; Han, B.; Huang, S.; Kadish, K. M. *Inorg. Chem.* **1996**, *35*, 3012−3021.
(44) Bear, J. L.; Wellhoff, J.; Royal, G.; Van Caemelbecke, E.; Eapen, S.; Kadish, K. M. *Inorg. Chem.* **2001**, *40*, 2282−2286.